Determining the anisotropic interaction potential of D_2Ar from rotationally inelastic cross sections

U. Buck and H. Meyer
Max Planck Institut für Strömungsforschung, D 3400 Göttingen, Federal Republic of Germany

R. J. LeRoy
Guelph-Waterloo Centre for Graduate Work in Chemistry, University of Waterloo, Waterloo, Ontario, Canada N2L 3G1

(Received 9 December 1983; accepted 14 February 1984)

In a crossed molecular beam experiment, time-of-flight distributions of oD_2 molecules scattered from Ar have been measured in a center-of-mass angular range from 50° to 100° at a collision energy of $E = 85$ meV. The data show clearly resolved 0→2 rotational transitions of D_2 in the backward direction. From a combined analysis of these inelastic cross sections and the measured total differential cross sections for $D_2 + Ar$ at $E = 83$ meV, the complete repulsive potential surface is derived. Comparison with the potential which LeRoy and Carley determined from spectroscopy shows that the repulsive part of its anisotropic V_2 term is steeper, whereas the isotropic parts V_0 agree within the experimental error. A combined analysis of the present inelastic scattering data and the original spectroscopic data yields an improved version of the three-dimensional stretching-dependent potential surface of LeRoy and Carley. Cross sections calculated from the semiempirical "HFD" potentials reported by Tang and Toennies and by Rodwell and Scoles are also fairly close to experiment, with the latter potential performing somewhat better than the former. The comparison with other hydrogen molecule–rare gas interactions reveals a maximum in the effective strength of the repulsive anisotropy for $Ne–H_2$ and a nearly complete conformality of the reduced V_0 and V_2 terms to each other for He, Ne, and $Ar–H_2$.

I. INTRODUCTION

The hydrogen molecule–rare gas systems have been extensively investigated during the past ten years as prototypes of systems with weakly anisotropic potential energy surfaces. Some of them are simple enough to be accurately described by *ab initio* electronic structure calculations with full configuration interaction,[1] and all may be realistically approximated by "Hartree–Fock dispersion" (HFD) model potentials[2,3] in which SCF calculations for the short range repulsion are combined with suitably damped dispersion coefficients which give rise to the potential well. At the same time, many types of experimental data are available and have been analyzed in terms of potential functions. In particular, molecular beam measurements of the velocity dependence of integral cross sections[4–7] and of total differential cross section,[8] virial coefficients,[9] and high precision diffusion data[10,11] have been used in this way. However, most of these data are only sensitive to the effective spherical part of the potential. Information on the potential anisotropy, has been obtained from nuclear magnetic resonance relaxation times,[12] integral cross sections of oriented molecues,[13] infrared absorption spectroscopy[14–16] and molecular beam magnetic resonance spectroscopy[17] of van der Waals molecules.

Most of the data mentioned above are sensitive mainly to the attractive part of the potential. However, state selective elastic and rotationally inelastic large angle differential scattering cross sections are a particularly direct tool for probing the repulsive part of both the isotropic and the anisotropic part of the potential surface. Moreover, a complete two-dimensional potential surface of $Ne + D_2$ derived mainly from the differential cross sections of 0→0 and 0→2 rotational transitions[18] is also able to predict correctly the differential cross sections of 0→1 transitions of HD,[19] the velocity dependence of the integral cross sections of oriented molecules[13] and the diffusion coefficient.[10,11] The present contribution reports similar results for $Ar + D_2$. Total differential cross sections were obtained at a collision energy $E = 83.0$ meV in the center-of-mass (c.m.) angular range from 3° to 100°. For three selected angles in the backward direction we also measured the 0→2 rotational transitions at a slightly different energy $E = 85$ meV (Sec. II).[20] A preliminary evaluation of these data has appeared elsewhere.[21]

In the present work these data have been used, together with some theoretical constraints on the attractive part of the potential and results from spectroscopy,[16] to devise a complete *two*-dimensional potential surface. This yields the first reliable potential for the repulsion anisotropy of this system based on experimental data (Sec. III). These results are compared with predictions of two of the HFD type model potentials which have been proposed for this system (Sec. IV).

Another comparison is made with the most reliable potential previously reported for this system, the "BC_3 function" of LeRoy and Carley.[16] This surface is unique in that it is three dimensional, incorporating a dependence on the hydrogen bond length as well as on the other two degrees of freedom. It was derived from a careful analysis of the discrete infrared van der Waals molecule spectra of McKellar and Welsh[22] with a collapsed diatom limit constraint imposed on the potential. This surface is in close agreement with results derived from total differential cross sections,[8]

 0021-9606/84/115589-09$02.10

low energy integral cross sections with orbiting resonances,[6] and integral cross sections for oriented molecules[13] (Sec. V). Its isotropic part is also fairly consistent with our data, but the anisotropy strength function is found to be too steep in the repulsive region. A combined analysis of the present inelastic scattering data and the original spectroscopic data is therefore used here to yield an improved version of the BC_3 three-dimensional surface.

Finally, we compare the results of the present work with the anisotropic potential surfaces for hydrogen molecules interacting with other rare gases, and in particular with the accurately known potentials for $He + H_2$ (Ref. 1) and $Ne + H_2$ (Ref. 18), as well as with the earlier spectroscopic potentials obtained[14] for $Kr + H_2$ and $Xe + H_2$ (see Sec. VI). Regularities and general trends for the anisotropies and the reduced potentials forms are discussed for these systems.

II. EXPERIMENTAL RESULTS

A. Apparatus

The details of the molecular beam machine are discussed elsewhere.[18,23] Briefly, the D_2 and Ar beams are produced as nozzle beams in two differentially pumped source chambers. They are introduced into the scattering chamber through skimmers which define beams with small angular divergence. At the scattering center the two beams cross at an angle of 90°. The angular dependence of the cross section is measured by rotating the source assembly relative to the scattering center. Scattered particles are detected by a universal detector containing an ionizing source, a quadrupole mass filter and secondary electron multiplier. Single inelastic transition probabilities are determined by measuring the flight time of the scattered particles by means of the pseudorandom chopping technique.

The argon is expanded at low pressure through a large nozzle to avoid condensation and to obtain a reasonable intensity. For the D_2 gas, condensation effects do not need to be considered. The D_2 gas is fed through a converter which produces *ortho* D_2 (oD_2) in which only states with even rotational quantum numbers are populated. On expanding the oD_2 gas at high pressure, nearly all D_2 particles are found in the ground rotational state $j = 0$.

Thus, the time-of-flight (TOF) spectra are measured with oD_2, while the total differential cross sections are measured with normal D_2 (nD_2), which is only 67% *ortho*. The beam parameters are listed in Table I. The degree of rotational excitation of the initial D_2 beam is estimated by extrapolation from Raman studies of nozzle beams at lower stagnation pressures.[24]

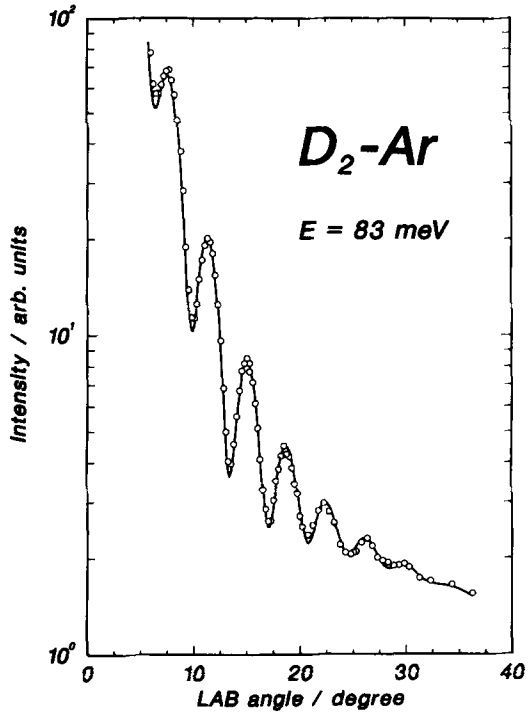

FIG. 1. Measured total differential cross sections in the laboratory system. The solid line is calculated from the present best-fit potential of Table III.

B. Experimental results

The total differential cross sections measured at a relative kinetic energy of 83.2 meV are shown in Fig. 1. Since the potential well depth of this system is small compared to the collision energy, only well resolved diffraction oscillations are observable. The angular positions of these oscillations, which are a direct measure of the position of the repulsive wall of the interaction potential, have experimental uncertainties of only 0.2%, whereas the large angle nonoscillatory cross section is known only to about 10%.

TABLE I. Beam parameters.

	nD_2	Total	Ar	oD_2	TOF	Ar
Energy (meV)			83.0			85.0
Velocity (m/s)	2017		565	2042		560
Nozzle diameter (μ)	20		100	10		50
Source pressure (bar)	100		1.8	192		3
Source temperature (K)	...		...	304		304
Speed ratio (S)	29.6		22	29		21
Beam divergence (deg)	1.6°		3.4°	1.7°		4.0°
Rotational temperature (K)	...		...	70		...
Population in $j = 0$	...		...	0.89		...
$j = 2$	...		...	0.11		...

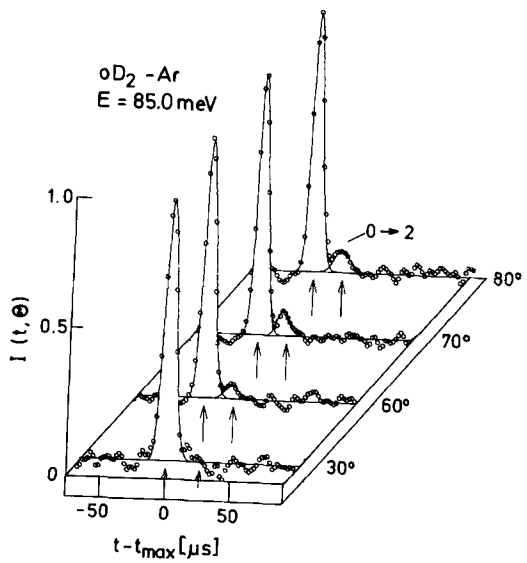

FIG. 2. Measured time-of-flight distributions of oD_2 + Ar for different laboratory scattering angles. The peaks correspond to the elastic (normalized to 1) and the inelastic $j = 0 \rightarrow 2$ rotational transitions.

Time-of-flight spectra have been measured at laboratory (LAB) angles of $\theta = 40°$, 60°, 70°, and 80° for a collision energy $E = 85$ meV. The results are shown in Fig. 2. These spectra have been normalized relative to their maximum peak intensity after subtracting out a large background contribution. The large peak corresponds to elastic scattering while the smaller second peak at an energy loss of $E = 22.2$ meV is due to the $j = 0 \rightarrow 2$ rotational transition. The latter peak appears only at the larger deflection angles and increases in size with increasing angle. Because of background problems, the precision with which the relative magnitude of the inelastic peaks may be determined varies between 12% and 20% (see Table II).

C. Data analysis

The conversion of the data from laboratory time-of-flight measurements to center-of-mass differential cross sections follows closely the procedure described in detail in Ref. 18 and 25. First, the distribution functions of the final laboratory velocity $G_{if}(v_f)$ are calculated for all transitions $j = i \rightarrow f$ by a Monte Carlo procedure using as input data the measured angular and velocity spreads of the two beams and the transmission function of the time-of-flight analyzer. The intensity of the TOF spectrum is given by

$$N(\theta, v_f) = \sum_{if} K \cdot v_f^{-1} \overline{J}_{if} G_{if}(v_f) \cdot p_i \sigma_{if}(\bar{\vartheta}, \bar{g}). \quad (1)$$

K is a constant which depends only on angular variables, p_i is the fractional initial state population, σ_{if} is the differential cross section, and J_{if} the Jacobian of the transformation from the center of mass to the LAB system. The bars indicate variables averaged over the small distribution functions. The summation has to be carried out over all possible transitions, included those which lead to the same energy loss.

In a second step the calculated distribution functions are fitted to the measured spectra, the only adjustable parameter being the amplitude. With the known values for v_f and J_{if} we get from the spectra the cross sections at the energy loss ΔE (in meV):

$$\sigma(\Delta E = 0) = K(p_0\sigma_{00} + p_2\sigma_{22}),$$
$$\sigma(\Delta E = 22) = K p_0 \sigma_{02}. \quad (2)$$

Using the values from Table I for p_i and the identity $\sigma_{00} + \sigma_{02} = \sigma_{22} + \sigma_{24} \approx \sigma_{22}$ we can easily derive the relative cross sections $K\sigma_{02}$ and $K\sigma_{00}$. To determine absolute values, the constant K has to be determined. This is done by adjusting the total differential cross section (which contains the same constant) to agree with a calculation based on a reliable interaction potential. The values given in Table II are based on the best-fit potential of this work (see Table III).

III. FITTING PROCEDURE AND POTENTIAL DETERMINATION

The main objective of the present study is the determination of a reliable anisotropic potential from the rotationally inelastic scattering data. The interaction potential is expanded in terms of Legendre polynomials

$$V(R, \gamma) = V_0(R) + V_2(R) P_2(\cos\gamma) + \cdots, \quad (3)$$

where R is the distance between the atom and the center of mass of the molecule and γ is the angle between the molecular axis and **R**. For the energy and the transition under investigation, it is sufficient to truncate this series after the first angle-dependent term. *Ab initio* calculations for hydrogen molecule–rare gas systems show that the V_4 term is not larger than 7% of the V_2 term.[1] If such a small V_4 term is included in the calculation of the scattering cross sections, the $0 \rightarrow 2$ transition changes by less than 2% justifying the neglect of this contribution.[18] Similar conclusions have been obtained from the analysis of infrared spectra.[26]

Detailed model studies show that $V_2(R)$ can be determined to a high accuracy from cross sections for the $j = 0 \rightarrow 2$ transition only if the isotropic part $V_0(R)$ is well known, since this part determines the range of $V_2(R)$ which is probed.[18,21] We therefore begin by obtaining a reliable effective spherical part of the potential.

TABLE II. Measured differential cross sections for the rotational excitation of D_2 in D_2 + Ar collisions at $E = 83$ meV. ϑ_{if} are c.m. scattering angles for the transition $i \rightarrow f$. The absolute values are obtained by calibrating the elastic cross sections by calculation based on the best fit potential of this work.

θ(LAB)	ϑ_{02}	$\sigma_{02}/\text{Å}^2\,\text{sr}^{-1}$	ϑ_{00}	$\sigma_{00}/\text{Å}^2\,\text{sr}^{-1}$
60°	72.2°	0.136(±0.027)	72.7°	2.259(±0.045)
70°	72.2°	0.174(+0.019)	85.5°	1.935(±0.039)
80°	98.8°	0.181(±0.022)	98.3°	1.734(±0.035)

TABLE III. Characteristic parameters of various potentials for Ar + D_2.

	V_0					V_2			
	Ref.	ϵ/meV	R_m/Å	R_0/Å	$V_0(2.7)$/meV	ϵ/meV	R_m/Å	R_0/Å	$V_2(2.7)$/meV
Tang, Toennies	2	6.30	4.58	3.196	98.5	0.645	3.73	3.34	20.0
Rodwell, Scoles	3	6.45	3.57	3.164	69.5	0.751	3.72	3.32	16.3
LeRoy, Carley ($k=0$)	16	6.307	3.573	3.171	82.8	0.709	3.743	3.34	20.3
Vib.av. ($J=0, v=0$)	16	6.256	3.573	3.172	82.3	0.698	3.744	3.35	20.1
This work ($m=3.022$)		6.30	3.578	3.173	76.5	0.711	3.725	3.34	21.1

The potential model used is the generalized Buckingham–Corner form introduced by LeRoy and Carley[16]

$$V_\lambda(R) = A_\lambda R^{-m_\lambda}\exp(-\beta_\lambda R) - (C_{6\lambda}R^{-6} + C_{8\lambda}R^{-8})f(R), \quad (4)$$

where

$$f(R) = \exp[-4(R_{d\lambda}/R - 1)^3] \quad \text{for } R < R_{d\lambda}$$
$$= 1 \quad \text{for } R \geqslant R_{d\lambda}.$$

There are six free parameters for each potential $\lambda = 0,2$. Two of them, usually A_λ and $C_{8\lambda}$, can be replaced by the characteristic minimum depth and position parameters ϵ_λ and $R_{m\lambda}$.[27] The parameters of the damping function $R_{d\lambda}$ are set equal to the corresponding minimum distances $R_{m\lambda}$. The remaining parameters are determined as follows.

The $C_{6\lambda}$ are fixed at calculated values[16] and ϵ_λ and $R_{m\lambda}$ are allowed to vary only within the error limits given by LeRoy and Carley.[16] Then we are left with two shape parameters for the repulsion β_λ and m_λ. For the isotropic part they are determined from the positions of the diffraction oscillations of the total differential cross section, which are to a high precision a measure of the distance at which the isotropic part equals zero, R_{00}, plus the large angle scattering which determines the steepness of the potential. An attempt to use the simpler $m_\lambda = 0$ version of this potential form failed, since the best-fit potential-minimum parameters obtained (when only differential cross sections were used as input information) were outside the error limits given by spectroscopy (see Ref. 21). The complete potential form of Eq. (4) was therefore used. For $V_2(R)$ we use the m value obtained for the isotropic potential and determine β_2 from the inelastic cross sections. The parameters resulting from a simultaneous best fit to both types of cross sections, using the full potential surface (see Ref. 18), are as follows:

$$A_0 = 1811.95 \text{ eV}, \quad A_2 = 604.13 \text{ eV},$$
$$C_{60} = 16.676 \text{ eV Å}^6, \quad C_{62} = 1.6738 \text{ eV Å}^6,$$
$$C_{80} = 128.51 \text{ eV Å}^8, \quad C_{82} = 27.77 \text{ eV Å}^8,$$
$$\beta_0 = 4.584 \text{ Å}^{-1}, \quad \beta_2 = 4.75 \text{ Å}^{-1}, \quad (5)$$
$$m_0 = m_2 = -3.022.$$

The characteristic strength and length parameters of the best-fit potential described by Eqs. (3)–(5) are summarized in Table III, together with analogous constants for previously proposed potentials. Comparisons of calculations based on this potential with the experimental results for the diffraction oscillations and the large angle part of the total differential cross section are shown in Figs. 1 and 3, respectively. The corresponding state selected cross sections for 0→0 and 0→2 transitions are displayed in Fig. 4; the present best-fit-potential yields the solid curves. The agreement is, in all cases, nearly perfect. The dimensionless standard deviations (DSD, as defined in Ref. 16 or 18) associated with this fit are given in Table IV. In conclusion, the total differential cross sections are only consistent with potentials having a zero at $R_{00} = 3.175(\pm 0.002)$ Å and an isotropic potential strength at $R = 2.7$ Å of $V_0(2.7) = 77(\pm 10)$ meV.

As a further test of the reliability of this potential, we have calculated the second virial coefficient and the diffusion coefficient. The second virial coefficients for the interaction of an atom and a diatom are given by (where $\beta = 1/kT$)[28]

$$B_{12}(T) = \pi N_L \int dR\, d(\cos\gamma) R^2 [1 - \exp(-\beta V(R,\gamma))]. \quad (5)$$

To include the anisotropy of the potential in a suitable form, the Legendre expansion of Eq. (3) is used and the exponential function is expanded in powers of β, yielding

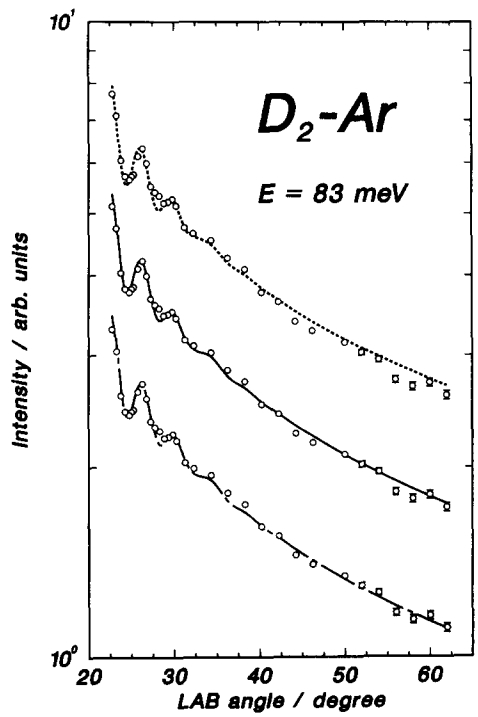

FIG. 3. Comparison of measured large angle total differential cross sections with calculations based on three different potential:—this work; ---Tang and Toennies (Ref. 2);—Rodwell and Scoles (Ref. 3). The curves are arbitrarily shifted from each other.

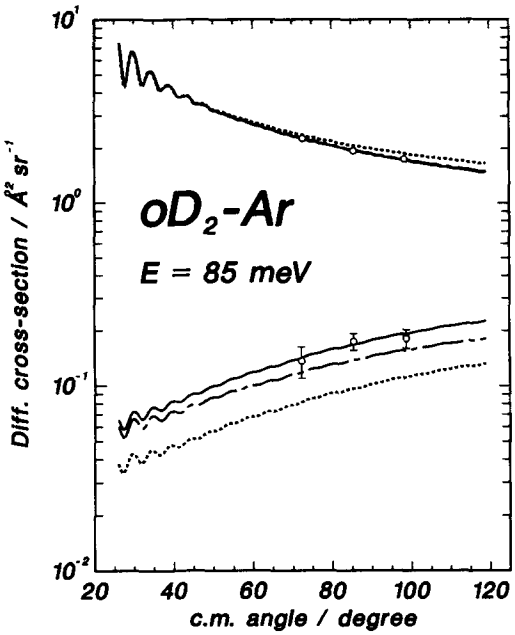

FIG. 4. Comparison of measured differential cross sections for 0→0 (upper curves) and 0→2 (lower curves) rotational transitions of oD_2 + Ar with calculations based on three potentials (see Fig. 6).

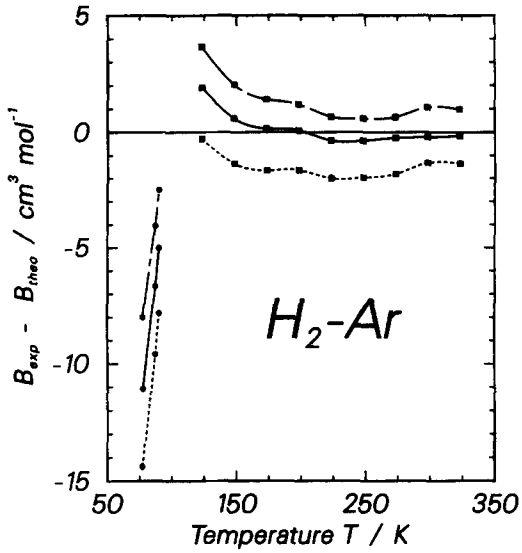

FIG. 5. Comparison of measured second virial coefficients (● Ref. 9, ■ Ref. 28) with calculations based on the three potentials of Fig. 6.

$$B_{12}(T) = 2\pi N_L \left\{ \int dR\, R^2 [1 - \exp(-\beta V_0)] - \sum_{n>1} (-1)^n \beta^n (n!)^{-1} \times \int dR\, R^2 \exp(-\beta V_0) [V_2(R)]^n \langle P_2(\cos\gamma)^n \rangle \right\}. \quad (6)$$

The brackets surrounding $P_2(\cos\gamma)^n$ in the last term denote the averaging over all orientation angles γ. The calculations show that the largest contribution to $B_{12}(T)$, the first term in Eq. (6), is caused by the isotropic part of the potential, while the term depending on the anisotropy yields only small corrections which decrease with β^n. The latter contributions are also small compared to the first radial quantum corrections, which has also been included in the calculation. The $B_{12}(T)$ values calculated using the present potential are compared with experimental results of Brewer[29] and Schramm *et al.*[9] in Fig. 5. The calculated results are in excellent agreement with the high temperature experiments,[29] but they disagree with some of the low temperature measurements[9] by more the reported experimental uncertainty of ± 6 cm^3/mol.

The binary diffusion coefficient was calculated using the computer program of Pack (see Ref. 30). Although this procedure only takes account of the isotropic part of the potential, the validity of this approximation for this type of system has been demonstrated by a direct comparison with a full close coupling calculation for the case of H_2–Ne.[31] The calculation based on the best fit potential of this work gives $D_{12}(H_2 + Ar) = 0.816$ cm^2/s at $T = 300$ K, a result in reasonable agreement with the experimental value of 0.824 cm^2/s.[10,11]

IV. COMPARISONS WITH HFD MODEL POTENTIALS

The present section examines the two Hartree–Fock dispersion model potentials which have been proposed for this system by Tang and Toennies (TT)[2] and Rodwell and Scoles (RS),[3] and compares calculations based on them both with experiment and with calculations associated with the best-fit potential described above. These three potentials are shown in Fig. 6 and some characteristic parameters are given in Table III. Although the general behavior of the two HFD potentials is quite similar, they differ in a number of details.

For the four main types of quantities considered hitherto the root mean square deviations associated with the pre-

TABLE IV. Dimensionless standard deviations for predictions of various H_2/D_2 + Ar potentials.

Property	Potential of: Ref. 2 TT	Ref. 3 RS	Ref. 16 vib.av.	Ref. 21	This work Sec. III
Total diff., oscillations (this work)	0.88	1.66	1.16	0.60	0.98
Total diff., large angles (this work)	0.53	0.22	0.35	0.19	0.19
Diff. 0→2 (this work)	3.92	1.65	0.51	0.57	0.45
Virial coefficient (Refs. 9, and 29)	1.19	0.87	0.76	1.23	0.77

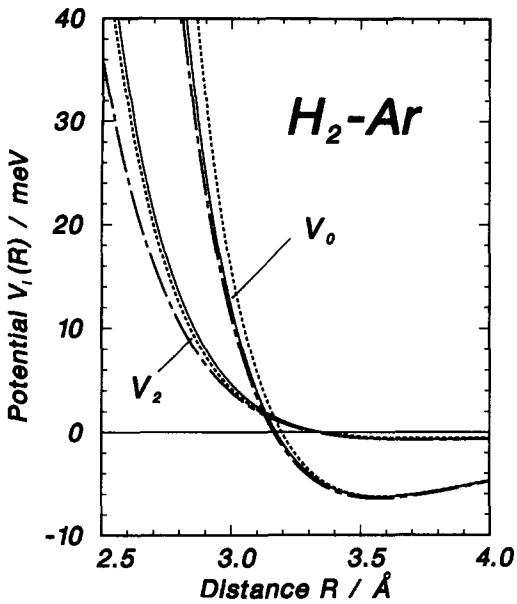

FIG. 6. Isotropic (V_0) and anisotropic (V_2) interaction potentials for $D_2(H_2)$–Ar:—this work; ---Tang and Toennies (Ref. 2);—·—Rodwell and Scoles (Ref. 3).

dictions of the various potentials are listed in Table IV. Detailed comparison of their ability to reproduce the experimental data are provided by Fig. 3 for the large angle total differential cross sections, and by Fig. 5 for the second virial coefficients. The most discriminating experimental quantity appears to be the rotationally inelastic $j = 0 \rightarrow 2$ cross section, with regard to which the predictions of both models are too small, with those for the TT model lying far outside the stated error bounds.

A comparison of the isotropic and anisotropic parts of the TT potential with those of our best fit potential clearly implies that the errors in the inelastic cross sections associated with the former occur because the repulsive part of $V_0(R)$ is too strong. This conclusion is also consistent with the deficiencies of the large angle elastic differential cross sections implied by the TT function (see Fig. 3). Conversely, for the RS model the anisotropy strength function $V_2(R)$ appears to be too weak; this leads to less dramatic discrepancies in the calculated inelastic cross sections since $V_2(R)$ grows at a slower rate than does $V_0(R)$ as R decreases. For the virial coefficients (see Fig. 5) the RS model again gives better results than does the TT model. In general, the predictive character of the two models is satisfactory if only moderate accuracy is required or if the measured quantities are not too sensitive to the potential. This qualitative agreement, achieved with no adjustable parameters, attests to the utility of the HFD-type procedure for estimating potential energy surfaces in the absence of other information. However, for special quantities like the $j = 0 \rightarrow 2$ excitation cross sections, their prediction can deviate appreciably, as is seen here for the TT model.

V. COMPARISONS WITH SPECTROSCOPIC POTENTIAL ENERGY SURFACE

The $BC_3(6, 8)$ function of LeRoy and Carley[16] is the most sophisticated and reliable potential energy surface previously derived for the Ar–H_2 system. It was obtained from an analysis of the discrete infrared spectra of the van der Waals molecules H_2–Ar and D_2–Ar,[22] subject to the constraints that it have the correct theoretical C_6 coefficients and the correct behavior in the "collapsed diatom limit" when H_2–Ar becomes He–Ar. This analysis determined not only the effective spherical and anisotropic radial strength functions $V_0(R)$ and $V_2(R)$, but also their dependence upon the diatom bond length. The radial potential strength function used had the form of Eq. (4) with $m_\lambda = 0$ and $R_{d1} = R_{d2} = R_{m0} = 3.5727$ Å used to define the onset of change in the damping function $f(R)$.

In addition to reproducing the spectroscopic data from which it was determined,[22] this potential surface is also able to predict correctly the low energy integral cross sections,[6] total differential cross sections,[8] and the integral cross sections of oriented molecules.[13] However, all of these phenomena are mainly sensitive to the attractive or near repulsive part of the potential outside its zero point. It is therefore very interesting to examine its ability to reproduce the present measurements, which are relatively more sensitive to the repulsive short-range part of the interaction.

A preliminary test[21] of the rigid diatom version of the isotropic part of this potential (denoted $k = 0$ in the nomenclature of Ref. 16) suggested that its zero point was slightly too small, since it could not fully account for the diffraction oscillations, and that its repulsive part was too steep, since it did not properly describe the diffusion coefficients[10,11] and large angle total differential cross sections. An attempt to take these effects into account by simply changing the common coefficient β of the exponential function gave predictions of the spectroscopic data which were far outside the experimental uncertainties. However, it was conceivable that these discrepancies could merely reflect the lack of proper vibrational averaging (over the diatom bond length) in the form of the potential used in those tests. The tests have therefore now been repeated using the proper vibrationally averaged version of this potential.

The diatom vibrational averaging referred to above, described in Ref. 32, was performed using the diatom bond length expectation values tabulated in Table IV of Ref. 16. Some of the resulting effective potential parameters for the $D_2(v = 0, j = 0)$ + Ar potential used in the present calculations are shown in Table III. For the isotropic potential, the vibrational averaging shifts the position of the zero R_{00} and the steepness to values in slightly better agreement with experiment, but some discrepancies still remain. This is demonstrated by the root mean square deviations in Table IV associated with the predictions of total differential cross sections and second virial coefficients. However, a careful inspection of the calculated quantities shows that they are very close to the calculations of the best fit "scattering potential" as shown in Figs. 3 and 5. The direct comparison of the two potentials reveals the same behavior. The potentials nearly coincide within the thickness of the lines shown in Fig. 6. Therefore we conclude that the vibrationally averaged $BC_3(6, 8)$ potential is essentially consistent with our experimental data.

Once a reliable effective $V_0(R)$ function is known, one

TABLE V. Calculated $j = 0 \rightarrow 2$ rotational excitation cross sections for D_2 + Ar at 85 meV in $Å^2$/sr.

θ/deg	BC_3 ($k = 0$)[a] Ref. 16	BC_3 (vib)[a] Ref. 16	BC_3 (vib) $\beta_2 = 4.20$ $Å^{-1}$	Best fit ($m = -3.022$)	Experiment
72.2	0.119	0.118	0.136	0.142	0.136(27)
85.4	0.140	0.139	0.165	0.168	0.174(19)
98.8	0.159	0.157	0.193	0.192	0.181(22)

[a] In the potential of Ref. 16, $\beta_0 = \beta_2 = 3.610$ $Å^{-1}$.

can easily calculate the differential inelastic cross sections to test the anisotropy of the short-range part of the given potential surface. This calculation was done here using the vibrationally averaged potential associated with $D_2(v = 0, j = 0)$; this approach is not completely correct since the process under study involves a transition from $j = 0$ to $j = 2$. However, in view of the relatively weak dependence of the vibrationally averaged potentials upon j, this should be a fairly good approximation. The inelastic cross sections obtained in this way are shown in Table V. The results obtained directly from the vibrationally averaged potential of Ref. 16 are clearly lower than the experimental values by more than the experimental uncertainty.[33] In order to achieve consistency with the inelastic cross sections, the short-range anisotropy of the ($v = 0$, $j = 0$) spectroscopic potential[16] must be strengthened.

In the analysis of the spectroscopic data in Refs. 14 and 16, the exponent coefficient β_2 was assumed to be the same for both the isotropic ($\lambda = 0$) and anisotropic ($\lambda = 2$) radial strength functions, because the available data were unable to determine them independently. An investigation of the sensitivity of that analysis to the parameters β_0 and β_2 showed that the infrared van der Waals molecule spectra are quite sensitive to the value of β_0, but scarcely at all to the value of β_2. We therefore repeated the fits to the spectroscopic data with the isotropic potential fixed as the function reported in Ref. 16, and determined the potential anisotropy associated with β_2 values ranging from 3.0 to 4.7 $Å^{-1}$. For this range of cases, the quality of fit to the spectroscopic data did not change significantly, but the agreement with the measured inelastic cross sections changed rather dramatically. The approach yielded anisotropy strength functions which, when combined with the isotropic potential of Ref. 16, are in excellent agreement with both spectroscopy and the present inelastic cross section measurements. The parameters defining the anisotropy of the resulting best-fit potential (see Ref. 16) are summarized in Table VI. Note that the values of Table VI contain all the information for deriving the vibrationally averaged potentials for different states of both isotope combinations. The associated parameters of the effective $V_2(R)$ function, vibrationally averaged for $D_2(v = 0, j = 0)$, are:

$\beta_2 = 4.20$ $Å^{-1}$[11] $\quad m_2 = 0$,
$A_2 = 2927.32$ eV, $\quad \epsilon_2 = 0.7054$ meV,
$C_{82} = 20.539$ eV $Å^8$, $\quad R_{m2} = 3.675$ Å,
$C_{62} = 1.644\,755$ eV $Å^6$.

Although ϵ_2 and R_{m2} are not very different from the values obtained from the spectroscopy alone,[16] the value of $V_2(R = 2.7\ Å) = 24.7$ meV is now some 23% larger than before, and this change yields a single potential which reproduces both the spectroscopy and the differential inelastic cross sections.

We therefore conclude, that with the isotropic potential fixed as the $\lambda = 0$ part of the $BC_3(6, 8)$ function of Ref. 16, optimum agreement with both spectroscopy and the present inelastic cross sections is obtained with the $\beta_2 = 4.2$ $Å^{-1}$ potential anisotropy of Table VI. While the shape of the repulsive part of the effective spherical potential is still slightly less than ideal as far as the total differential cross sections are concerned, this combined surface is in quite good agreement with these data, and is at present the best three-dimensional potential energy surface for this system. However, in future efforts to devise a further improved surface for this system, it seems clear that the second shape parameter m in Eq. (4) must be treated as a variable and not fixed at zero as it was in the previous (and present) analysis of the infrared spectroscopic data.

VI. COMPARISON WITH OTHER RARE GAS–HYDROGEN MOLECULE INTERACTIONS

With the availability of an Ar–H_2 potential with a reliable repulsive anisotropy, we are now in a position to compare this result with the Ne–H_2 potential derived from similar experimental sources[18] and with the theoretical He–H_2 potential of Ref. 1 (which agrees with the model of Ref. 3). The best available potential surfaces for Kr–H_2 and Xe–H_2

TABLE VI. Parameters defining the improved stretching-dependent $BC_3(6, 8)$ potential anisotropy which is consistent with both spectroscopy and scattering. The notation, potential form and isotropic ($\lambda = 0$) potential are those of Ref. 16. Energies are in cm^{-1}, lengths in Å; for all functions $\beta_2 = 4.20$ $Å^{-1}$ and $m = 0$.

	$\epsilon^{2,k}$	$R_e^{2,k}$	$C_6^{2,k}$	$A^{2,k}$	$C_8^{2,k}$
$k = 0$	5.79	3.674	13 500.0	23 920 216	167 884.8
1	26.7	3.8759	29 600.0	278 178 547	2 121 662.5
2	18.633	3.9314	5 705.0	254 258 331	1 953 777.8
3	...	...	− 10 395.0	0.0	0.0

TABLE VII. Parameters characterizing the potential minimum for rare gas–H_2 systems.

		He–H_2	Ne–H_2	Ar–H_2[a]	Kr–H_2	Xe–H_2
		Ref. 1	Ref. 18		Ref. 14	Ref. 14
V_0	ϵ_0/meV	1.20	2.85	6.30	7.29	8.12
	R_{m0}/Å	3.40	3.30	3.58	3.73	3.93
V_2	ϵ_2/meV	0.11	0.27	0.71	1.10	1.24
	R_{m2}/Å	3.60	3.56	3.73	3.86	3.98
R_{m2}/R_{m0}		1.059	1.079	1.041	1.038	1.012
ϵ_2/ϵ_0		0.092	0.095	0.113	0.151	0.153

[a] This work, see Sec. III and Table III.

are only expected to be reliable for the attractive part of the potential since they are derived essentially from spectroscopic data.[14] The parameters of the corresponding potential minima for V_0 and V_2 are presented in Table VII. For Ar–H_2 the potential derived in Sec. III is used. The general structure of the potential surfaces is quite similar. The potential well depth of the isotropic part is roughly a factor of 10 deeper than that of the anisotropic part, while in the repulsive region $V_2(R)$ is much weaker than $V_0(R)$. The absolute values of the potential well depth show the behavior expected from polarizability considerations, increasing with the mass of the rare gas atom. The position of the minimum decreases from Xe to Ne, but increases slightly from Ne to He, probably due to the anomalous weakness of interaction involving He.

A question of considerable interest is the trend in the relative anisotropies of these systems. In the attractive region this quantity may be expressed by the ratio ϵ_2/ϵ_0, which increases from 0.092 for He, over 0.095 for Ne, 0.113 for Ar, 0.151 for Kr and to 0.153 for Xe. The analysis of rotationally inelastic cross sections clearly shows that the strengths of the anisotropy $V_2(R)$ at the classical turning point of the isotropic repulsive wall $V_0(R)$ determines the inelastic transition probabilities in the backward direction. Values for a collision energy of $E = 0.1$ eV are given in Table VIII. The comparison shows the surprising result that the V_2 value, and thus the transition probability, is largest for Ne, reflecting essentially the fact that the Ne atom can penetrate much further toward the H_2 than can the larger Ar, Kr, and Xe and therefore "sees" a stronger anisotropy. This trend is not continued to He since the penetration is counterbalanced by weaker forces so that roughly the same inelasticity occurs for Ar and He. A similar behavior is also observed in the calculation of internal-rotation predissociation level widths, which are predicted to decrease from H_2–Ar to H_2–Kr to H_2–Xe, since they probe the same part of the potential.[32,34]

In order to illustrate the trends in shape and strength of the components of these potentials, Fig. 7 presents plots of $V_\lambda(R)/\epsilon_0$ vs R/R_{m0} for $\lambda = 0$ and 2. While the isotropic ($\lambda = 0$) functions all reduce to approximately the same form, particularly for He, Ne, Ar, and Kr, the same is not true for the reduced anisotropy strength functions. While there appears to be an easily-rationalized trend in the behavior of the reduced $V_2(R/R_{m0})$ function with increasing size of inert gas partner (see above), the H_2–Kr curve definitely appears to be out of order. Another perspective on the latter observation is provided by Table VIII, which compares the anisotropy strengths of the different surfaces at the turning point R_t on the corresponding isotropic potential associated with a collision at an energy of 0.1 eV. Figure 7 therefore illustrates both readily understood trends in the potential energy surfaces between H_2 and various inert gas partners, and the fact that the best available surfaces for H_2–Kr and H_2–Xe require significant further improvement. The latter fact should not be surprising, since these surfaces are distinctly older and/or less sophisticated than the best available surfaces for the other species.

TABLE VIII. Values of the anisotropy V_2 at the classical turning point R_t of the isotropic potential at the energy $E = 0.1$ eV for the H_2–rare gas systems.

	R_t/Å	V_2/meV
He–H_2	2.11	27.3
Ne–H_2	2.26	34.1
Ar–H_2	2.64	26.8
Kr–H_2	2.80	29.3
Xe–H_2	3.05	20.8

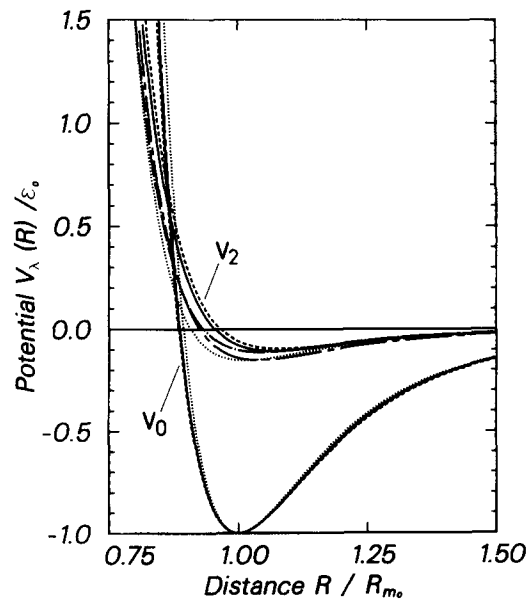

FIG. 7. Isotropic (V_0) and anisotropic (V_2) potential curves reduced by the isotropic potential minimum parameters for the H_2–rare gas systems.—He–H_2, ---Ne–H_2, -·-Ar-H_2,—Kr–H_2,···Xe–H_2.

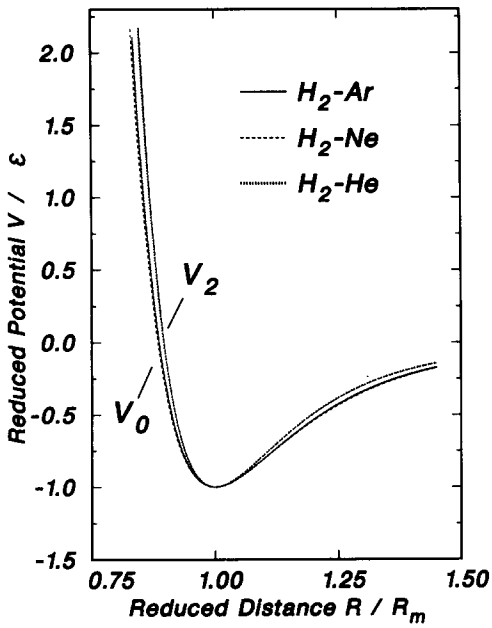

FIG. 8. Reduced potential terms for the H_2–Ar, Ne, He interactions. The potentials are taken from this work, Ref. 18, and Ref. 1, respectively.

Finally, the completely reduced potentials for $V_0(R)$ and $V_2(R)$ for H_2–He, Ne, Ar are compared in Fig. 8. In spite of the large differences of the size parameters and the partly anomalous behavior of He, the result is surprising. The potential shapes for $V_0(R)$ and $V_2(R)$ are nearly identical for the three systems, but differ from each other in that $V_2(R)$ is relatively a little steeper than $V_0(R)$. Note that this contrasts with the complete conformality found for the Tang–Toennies model.[2]

ACKNOWLEDGMENTS

We are grateful to Dr. R. T. Pack, Dr. J. M. Hutson, and Professor G. Scoles for their helpful comments on the manuscript. Computing time in Göttingen was supplied by the GWD, Göttingen.

[1]W. Meyer, P. C. Hariharan, and W. Kutzelnigg, J. Chem. Phys. **73**, 1880 (1980).
[2]K. T. Tang and J. P. Toennies, J. Chem. Phys. **68**, 5501 (1978); **74**, 1148 (1981).
[3]W. R. Rodwell and G. Scoles, J. Phys. Chem. **86**, 1053 (1982).
[4]K. Helbing, W. Gaide, and H. Pauly, Z. Phys. **208**, 215 (1968).
[5]H. P. Butz, R. Feltgen, H. Pauly, H. Vehmeyer, and R. M. Yealland, Z. Phys. **247**, 60 (1971).
[6]J. P. Toennies, W. Welz, and G. Wolfe, J. Chem. Phys. **71**, 614 (1972).
[7]R. Gengenbach and Ch. Hahn, Chem. Phys. Lett. **15**, 604 (1972).
[8]A. M. Rulis, K. M. Smith, and G. Scoles, Can. J. Phys. **56**, 753 (1973).
[9]B. Schramm, E. Elias, and R. Pilger, Chem. Phys. Lett. **88**, 459 (1982).
[10]R. D. Trengove and P. J. Dunlop, in *Proceedings of the Eighth International Symposium on Thermophysical Properties*, edited by J. V. Sengers (ASME, New York, 1981).
[11]R. D. Trengove and P. J. Dunlop, Ber. Bunsenges. Phys. Chem. **86**, 628 (1982).
[12]J. W. Riehl, C. J. Fisher, J. D. Baloga, and J. L. Kinsey, Chem. Phys. **58**, 457 (1973).
[13]L. Zandee and J. Reuss, Chem. Phys. **26**, 345 (1977).
[14]R. J. LeRoy, J. S. Carley, and J. E. Grabenstetter, Faraday Discuss. Chem. Soc. **62**, 169 (1977); J. S. Carley, *ibid.* **62**, 303 (1977).
[15]A. L. Dunker and R. G. Gordon, J. Chem. Phys. **68**, 700 (1978).
[16]R. J. LeRoy and J. S. Carley, Adv. Chem. Phys. **42**, 353 (1980).
[17]M. Waaijer and J. Reuss, Chem. Phys. **63**, 263 (1981).
[18]J. Andres, U. Buck, F. Huisken, J. Schleusener, and F. Torello, J. Chem. Phys. **73**, 5620 (1980).
[19]U. Buck, F. Huisken, J. Schlleusener, and J. Schaefer, J. Chem. Phys. **72**, 1512 (1980).
[20]J. Andres, U. Buck, F. Huisken, J. Schleusener, and F. Torello, in *Electronic and Atomic Collision*, edited by N. Oda and K. Takayanagi (North-Holland, Amsterdam, 1980), p. 531.
[21]U. Buck, Faraday Discuss. Chem. Soc. **73**, 187 (1982).
[22]A. R. W. McKellar and H. L. Welsh, J. Chem. Phys. **55**, 595 (1971).
[23]U. Buck, F. Huisken, J. Schleusener, and J. Schaefer, J. Chem. Phys. **72**, 1512 (1980).
[24]H. P. Godfried, I. F. Silvera, and J. van Straaten, *Twelfth International Symposium on Rarefield Gas Dynamics* (Am. Inst. Aeronautics and Astronautics, Charlottesville, Virginia, 1980), p. 772.
[25]U. Buck, F. Huisken, A. Kohlhase, D. Otten, and J. Schaefer, J. Chem. Phys. **78**, 4439 (1983).
[26]R. J. LeRoy and J. van Kranendonk, J. Chem. Phys. **61**, 4750 (1974).
[27]See Eqs. (74) and (75) of Ref. 16, with the correction that D_1 should actually be defined as: $D_1 = \{\partial \ln [D(R)]/\partial R\}_{R=R_d}$ and $R_d = R_{m0}$.
[28]J. O. Hirschfelder, C. F. Curtis, and R. B. Bird, *Molecular Theory of Gases and Liquids* (Wiley, New York, 1954), p. 153.
[29]J. Brewer and G. W. Vaughn, J. Chem. Phys. **50**, 2960 (1969).
[30]G. A. Parker and R. T. Pack, J. Chem. Phys. **68**, 1585 (1978).
[31]F. R. McCourt, Faraday Discuss. Chem. Soc. **73**, 280 (1982).
[32]R. J. LeRoy, G. C. Corey, and J. M. Hutson, Faraday Discuss. Chem. Soc. **72**, 339 (1982).
[33]The improved agreement with the data reported in Ref. 21 is erroneous for two reasons. First, the potential was coded incorrectly in that the scaling length used for the $\lambda = 2$ damping function was assumed to be R_{m2} rather than R_{m0}; secondly, the vibrational averaging was not taken into account.
[34]R. J. LeRoy, Farraday Discuss. Chem. Soc. **73**, 280 (1982).